A 3D FEM Study on the Axial Compressive Behavior of Normal Concrete Composite Square Columns with UHPC Internal Core

Thanh Vy Nguyen
Tra Vinh University, Tra Vinh City, Vietnam | University of Transport Ho Chi Minh City, Vietnam
thanhnv.NCS@ut.edu.vn

Tuan Anh Nguyen
University of Transport Ho Chi Minh City, Vietnam
tuanna@ut.edu.vn (corresponding author)

An Hoang Le
University of Transport Ho Chi Minh City, Vietnam
hoangan.le@ut.edu.vn

Received: 30 March 2025 | Revised: 16 May 2025, 5 June 2025, and 19 June 2025 | Accepted: 21 June 2025

 DOI: https://doi.org/10.48084/etasr.11217

ABSTRACT

This study uses the ABAQUS platform to develop a three-dimensional Finite Element Model (3D FEM) and analyze the axial compressive behavior of square composite columns consisting of Normal-Strength Concrete (NSC) with embedded Ultra-High-Performance Concrete (UHPC) cores. This study uses a complete 3D modeling approach that considers key parameters, such as the core shape, number of cores, and steel fiber content within the UHPC, in contrast to most existing research, which focuses on experimental studies on two-dimensional simulations. The simulation results strongly agree with the experimental data regarding the crack patterns, compressive strength, and deformation behavior. Additionally, a parametric analysis was conducted in ABAQUS to examine how UHPC core strength and thickness influence the structural performance. This approach offers a practical and efficient solution for assessing structures where experimental data are limited—a common issue in the existing literature.

Keywords-ultra-high performance concrete; structural applications; composite columns; ultra-high performance fiber reinforced concrete

I. INTRODUCTION

UHPC and Ultra-High-Performance Fiber-Reinforced Concrete (UHPFRC) are materials with great strength, high ductility, and low permeability [1-3], which are used for infrastructure construction, retrofitting, and strengthening deteriorated concrete structures. UHPC's bond capacity with NSC makes it an optimal choice for repair and reinforcement applications. The objective of this study is to develop a reliable model for predicting the axial compression behavior of normal concrete composite square columns with an internal UHPC core. Finite Element Analysis (FEA) is a useful tool for studying the composite UHPC-NSC structures and for designing them to enhance the strength and repair capacity. The ABAQUS software, which is known for its speed and versatility in simulating loading, thermal, and vibration problems, optimizes the analysis of concrete columns under compression using the Concrete Damage Plasticity (CDP) model, which is suitable for high-strength or NSC. Authors in [4] found that FEM of the interface behavior between NSC and UHPFRC is critical for predicting the strengthening and repair capabilities of structural elements. The researchers developed a surface-based cohesive model that employs a linear traction–separation law and calibrated its parameters using previous experimental data [5, 6]. Seven FEM simulations were applied to the shear, tensile, and flexural tests. The results demonstrated the model's effectiveness in the design and application of UHPFRC and UHPFRS systems, yielding low deviations: 6.8% in the peak load for the shear tests and 15.9% and 2.8% in the maximum displacement for the tensile and flexural tests, respectively. However, this model is limited to simple configurations and does not account for the variations in the core geometry, fiber distribution patterns, or multi-core interaction effects within the UHPC materials. Therefore, comprehensive FEM models capable of simulating the full structural behavior of the UHPC-NSC composite systems are necessary. Authors in [7] used ABAQUS software to simulate the behavior of UHPFRC columns under axial and eccentric loading, employing 2D and 3D FEM. The simulation results showed strong agreement with the experimental data [8-11], confirming that UHPFRC significantly enhances ductility and increases the ultimate load capacity compared to NSC and High-Strength Concrete (HSC). Furthermore, the proposed analytical model demonstrated acceptable accuracy for practical design applications. However, the study has limitations because it focuses on homogeneous UHPFRC columns and does not include critical factors, such as the dispersed core structures, fiber distribution effects, and variations in core geometry, in the parametric analysis. Additionally, the research did not fully explore the potential of FEM as an efficient predictive tool under conditions of limited experimental data—an important direction for advancing the application of the emerging material technologies. Authors in [12] proposed a 3D FEM using ABAQUS to examine the behavior of UHPFRC-filled steel tubular columns under axial and eccentric loading. This model's integration of critical practical factors, including the material limitations of UHPFRC, initial local and global geometric imperfections, and surface-to-surface interaction between the concrete core and the steel tube, was a major improvement [13–17]. The FEM predictions showed excellent agreement with the experimental data regarding the peak load capacity, failure patterns, and post-cracking behavior. Additionally, the analysis demonstrated that the UHPFRC cores are highly effective under axial and small eccentric loads and that enhancing the flexural performance involves increasing the steel's tensile strength and optimizing the diameter-to-thickness ratio. However, the study was limited to single-core, homogeneous columns. The present research aims to advance this approach by developing a more comprehensive 3D FEM capable of predicting the behavior of UHPC–NSC composite columns with complex geometries under realistic structural conditions. Most studies on UHPC and UHPFRC columns have focused on the experimental axial compression, while the numerical simulations are limited. This has created a significant gap in understanding and predicting the mechanical behavior of UHPC-based composite structures. Current simulation models often fail to capture the interactions between materials and the overall deformation behavior of the square composite columns with internal UHPC cores. This study seeks to minimize this gap by developing FEM on the ABAQUS platform to simulate the axial compressive behavior of the UHPC–NSC composite columns. These models were calibrated and validated using previous experimental data, showing good agreement regarding the crack patterns, compressive strength, and deformation characteristics. Additionally, a simplified model was developed to overcome the limitations of the experimental data under constrained testing conditions. The findings show that the usage of UHPC cores is a promising solution for strengthening the existing concrete structures.

II. MATERIAL MODEL AND METHODOLOGY

A. Finite Element Model and Meshing

The C3D8R solid element, an eight-node, linear brick element with reduced integration and hourglass control, is used for simulations and serves as the FEM for each material type in different structures. Previous studies have also adopted the the C3D8R element for the cores and shells of the columns under examination due to its computational efficiency and convergence properties. Owing to the experimental limitations in Vietnam, specifically the restricted height capacity of the compression testing machine and the limited mixing volume of the UHPC mixer (10 lt per batch), short column specimens with dimensions of 200 mm × 200 mm × 320 mm were selected to ensure experimental feasibility, as shown in Figure 1. Table I presents the number of specimens, core dimensions, core shapes, and steel fiber contents.

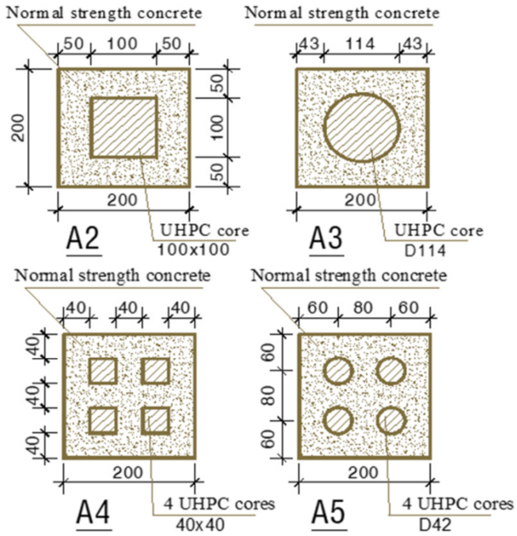

Fig. 1. UHPC-NSC test specimen cross section.

TABLE I. DETAILS OF SPECIMEN GROUPS

Spec. type	Spec. size		UHPC core size		Steel fibers	No. of Spec.	Note
	B, *D* (mm)	*H* (mm)	*b*, *d* (mm)	*h* (mm)			
A1	D100	200	-	-	-	3	Control sample
A2	200×200	320	100×100	320	0%, 1%, 2%	3, 3, 3	Fig.1
A3	200×200	320	d114	320	0%, 1%, 2%	3, 3, 3	Fig.1
A4	200×200	320	40×40	320	1%	3	Fig.1
A5	200×200	320	d42	320	1%	3	Fig.1

The FEM was based on the experimental setup and four specimen cases were considered, accounting for variations in the core shape, number of cores, and steel fiber content within the cores. Specimen models were used to ensure accurate meshing, and the mesh configuration was selected, as portrayed in Figure 2. The research findings suggest that in order to achieve reliable results, the element size should be approximately B/15 in the cross-sectional direction and L/20 along the longitudinal axis.

B. Material Model and Stress-Strain Relationship

The CDP model can simulate the concrete behavior from the pre-cracking stage through the post-cracking and ultimate failure [18], using the concept of the plastic damage in concrete after it reaches maximum compressive and tensile stress levels. The ABAQUS uses this model to simulate the concrete and other quasi-brittle materials.

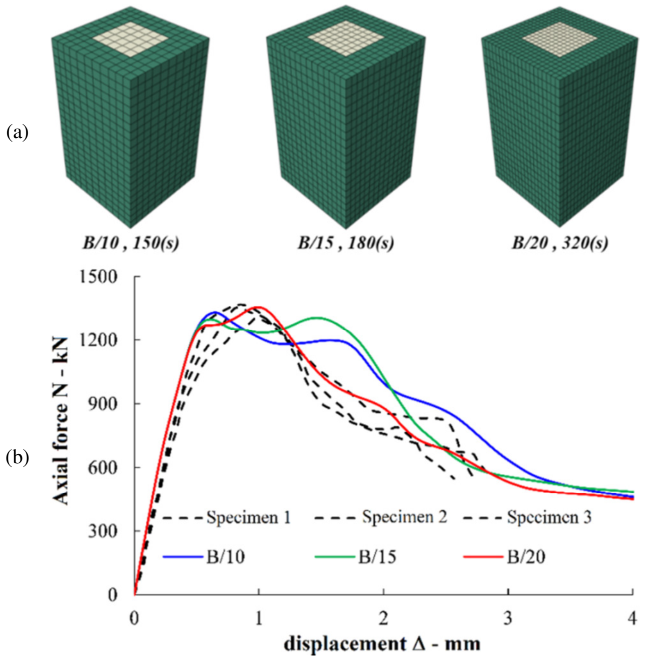

Fig. 2. (a) Specimens of different cross-sectional direction, (b) results of finite element meshing simulation.

The CDP model defines the stress-strain relationship of the concrete under compression and tension. Any point along the strain-softening branch shows a decrease in stiffness when unloaded. The parameters D_t and D_c characterize this stiffness degradation, where $D_t \geq 0$ and $D_c \leq 1$. In the CDP model:

- The behavior of concrete under tension is defined by the relationship between the stress and cracking strain.
- The behavior of concrete under compression is defined by the relationship between the stress and inelastic strain.

This relationship can be expressed as:

$$\varepsilon_c^{in} = \varepsilon_c - \frac{\sigma_c}{E_0} \quad (1)$$

$$\varepsilon_c^{ck} = \varepsilon_t - \frac{\sigma_t}{E_0} \quad (2)$$

for the compressive and tensile concrete, respectively.

C. Determination of Yield Surface and Material Parameters

The development of the yield surface is controlled by the variables $\varepsilon^{pl}{}_c$ and $\varepsilon^{pl}{}_t$. The yield surface function is:

$$F = \frac{1}{1-\alpha}\left[\bar{q} - 3\alpha\bar{p} + \beta(\varepsilon^{pl})\langle\bar{\sigma}_{max}\rangle - \gamma\langle-\bar{\sigma}_{max}\rangle - \bar{\sigma}_c(\varepsilon_c^{pl})\right] = 0 \quad (3)$$

where $\alpha = \frac{\left(\frac{\sigma_{b0}}{f_c'}\right)-1}{2\left(\frac{\sigma_{b0}}{f_c'}\right)-1}$, $\beta = \frac{\bar{\sigma}_c\left(\varepsilon_c^{pl}\right)}{\bar{\sigma}_t}(1-\alpha) - (1+\alpha)$, $\gamma = \frac{3(1-K_c)}{2K_c-1}$, $0 \leq \alpha \leq 0.5$, and $\bar{\sigma}_{max}$ is the maximum principal effective stress, $\frac{\sigma_{b0}}{f_c'}$ is the ratio of the initial biaxial compressive stress to the uniaxial compressive stress, K_c is the ratio of the second stress constant of the tensile part to that of the compressive part, with initial yielding of any constant value of pressure p, so that the maximum principal stress is negative ($\bar{\sigma}_{max} < 0$), and must satisfy the condition $0.5 \leq K_c \leq 1$. The default value in ABAQUS is 2/3 and, $\bar{\sigma}_t\left(\varepsilon_t^{pl}\right)$, $\bar{\sigma}_c(\varepsilon_c^{pl})$ are the effective fixed compressive and tensile stresses, respectively.

In order to apply the CDP model provided in ABAQUS, it is necessary to determine the following parameters:

1) Determination of Elastic Modulus (E_c) and Poisson's Ratio (μ)

The experimental formulas proposed in ACI 318 are used to calculate the elastic modulus E_c, where f_c' is measured in MPa. Moreover, the applied Poisson's ratio of 0.2 is frequently employed in simulation models:

$$E_c = 4700x\sqrt{f_c'} \quad (4)$$

2) Determination of the Ratio of Initial Biaxial Compressive Stress to Uniaxial Compressive Stress $\left(\frac{\sigma_{bo}}{f_c'}\right)$

The ratio of the initial biaxial compressive stress to the uniaxial compressive stress is $\left(\frac{\sigma_{bo}}{f_c'}\right)$. The results of the triaxial compression tests for normal concrete and HSC are based on a formula proposed in [19]:

$$\frac{\sigma_{bo}}{f_c'} = 1.5(f_c')^{-0.075} \quad (5)$$

3) Determination of the Ratio Between the Second Stress Invariant for Tension and Compression (K_c)

Determining the ratio between the second stress invariant for tension and compression (K_c) is one of the parameters used to define the yield surface of the CDP model. Authors in [20], showed that the range of K_c varies from 0.5 to 1and authors in [21] proposed a formula that is regarded as the most suitable approach for determining K_c in simulation problems:

$$K_c = \frac{5.5}{5+2x(f_c')^{0.0075}} \quad (6)$$

4) Determine the Expansion Angle of Concrete (Ψ)

The dilation angle is found to be significantly dependent on the strength of the concrete; as the strength of the concrete increases, the dilation angle also increases. Authors in [22], proposed dilation angles of 30° for concrete with strength below 60 MPa and 56° for concrete with strength above 90 MPa:

$$\begin{Bmatrix} \psi = 30^0 - NSC \\ \psi = 56^0 - UHPC \end{Bmatrix} \quad (7)$$

5) Determination of Stress-Strain

a) Behavior of NSC Concrete

The present study indicates that the concrete has a compressive strength below 50 MPa. Authors in [23] showed that the compressive behavior of NSC concrete is divided into two stages: the strengthening stage and the softening stage. In this context, $\varepsilon_{c,NSC}$ denotes the strain of the concrete when it attains the compressive strength f_c':

$$\frac{\sigma}{f_c'} = 2x\left(\frac{\varepsilon_c}{\varepsilon_{c,NSC}}\right) - \left(\frac{\varepsilon_c}{\varepsilon_{c,NSC}}\right)^2 ;\ 0 \leq \varepsilon_c \leq \varepsilon_{c,NSC} \quad (8)$$

$$\sigma = \frac{2xf_c' x\left(\frac{\varepsilon_c}{\varepsilon_{c,NSC}}\right)}{1+\left(\frac{\varepsilon_c}{\varepsilon_{c,NSC}}\right)^2}; \ \ \varepsilon_c > \varepsilon_{c,NSC} \quad (9)$$

Authors in [24] proposed a formula for determining $\varepsilon_{c,NSC}$ which is based on regression calculations with concrete specimens that have strengths ranging from 10 to 100 MPa:

$$\varepsilon_c = 0.00076 + \sqrt{(0.626xf_c' - 4.33)x10^{-7}} \quad (10)$$

Authors in [25] stated that the tensile behavior of concrete is examined for specimens with a compression strength of less than 50 MPa:

$$f_t = 0.3x(f_c')^{2/3} \quad (11)$$

In addition, the failure energy model for tensile concrete is proposed in [26]. d_{max} is defined as the maximum aggregate size in concrete:

$$G_{F,NSC} =$$

$$(0.0469xd_{max}^2 - 0.5xd_{max} + 26)x\left(\frac{f_c'}{10}\right)^{0.7} \quad (12)$$

b) Behavior of UHPC Concrete

In contrast to the behavior of NSC, UHPC demonstrates a distinct behavior due to its brittleness and susceptibility to sudden failure. Authors in [27] described the strengthening and softening behavior of concrete:

$$\frac{\sigma}{f_c'} = \frac{\beta x\left(\frac{\varepsilon_c}{\varepsilon_{c0}}\right)}{\beta - 1 + \left(\frac{\varepsilon_c}{\varepsilon_{c0}}\right)^{\beta}}; \ \beta = \frac{1}{1-\frac{f_c'}{\varepsilon_{c0}xE_c}} \quad (13)$$

$$\varepsilon_{c,UHPC} = (0.71xf_c' + 168)x10^{-5} \quad (14)$$

where $E_{c,\mathrm{UHPC}}$, and β are the strain corresponding to the point f_c' and the shape parameter, respectively.

III. RESULTS AND DISCUSSION

A. Failure Model Analysis

As presented in Figure 3, the simulation outcomes demonstrate that the column specimens (A2, A3, A4, and A5) exhibited distinctly disparate failure patterns. During the elastic stage, no surface abnormalities were observed. As the applied load approached 0.8 P_{max}, cracks began to form in the mid-height region and propagated toward the corners, exhibiting relatively large crack widths. However, for the columns with segmented UHPC cores (A4 and A5), the extent of damage was significantly reduced, although initial cracking still originated from the mid-height and spread along the perimeter. The results presented in Figures 4 and 5 show that the addition of steel fibers to the UHPC core did not have a substantial impact on the failure mode of the columns. It is noteworthy that the high degree of similarity between the simulation and experimental results with regard to the crack patterns and failure mechanisms validates the precision and dependability of the numerical model. Therefore, the FEM used in this study can be considered effective for predicting the load-bearing capacity of UHPC-NSC composite columns, supporting the practical applications in the structural design and evaluation.

B. Compressive Capacity Analysis

Figure 6 shows the compressive capacity of columns with different UHPC core configurations and steel fiber content. Increasing the fiber content from 0% to 1% for specimen A2 resulted in a 22.64% improvement in compressive strength. However, increasing the content to 2% led to a slight 3.28% reduction, suggesting a saturation point beyond the optimal fiber dosage. In contrast, Specimen A3 exhibited a 2.02% decrease in strength when the fiber content increased from 0% to 1%. Then, there was a 10.33% improvement when the content rose from 1% to 2%. These results suggest that the effectiveness of the steel fibers depends on their content and the configuration of the UHPC core.

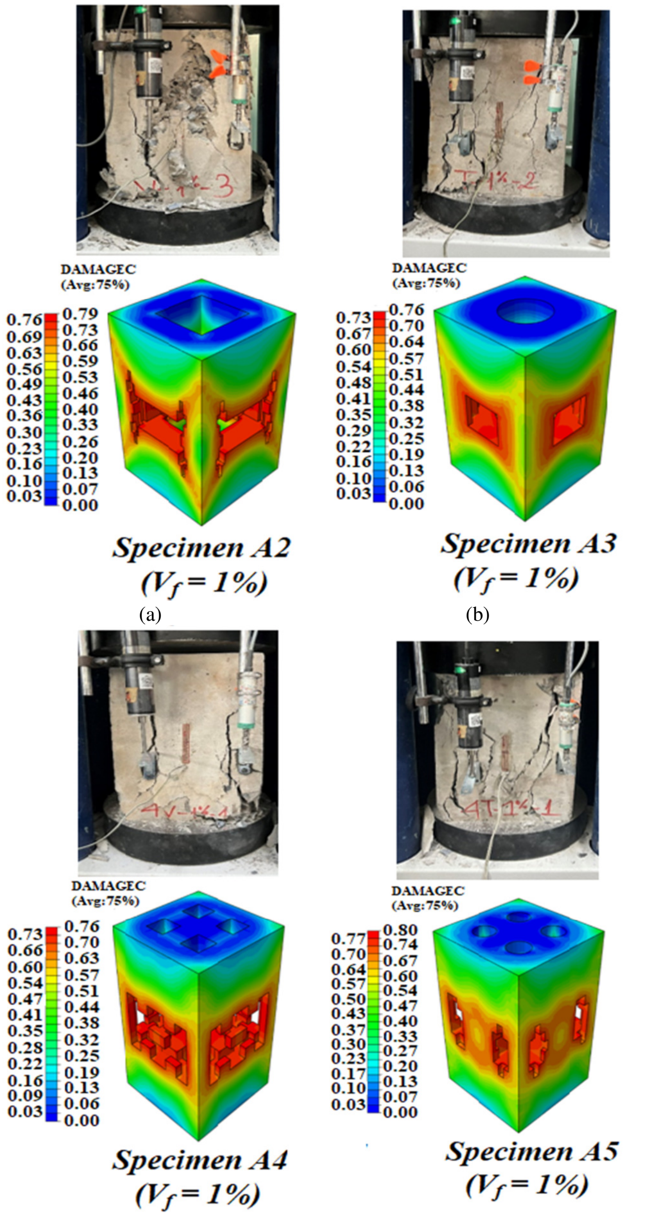

Fig. 3. Failure patterns of different column types: (a) specimen A2, (b) specimen A3, (c) specimen A4, (d) specimen A5.

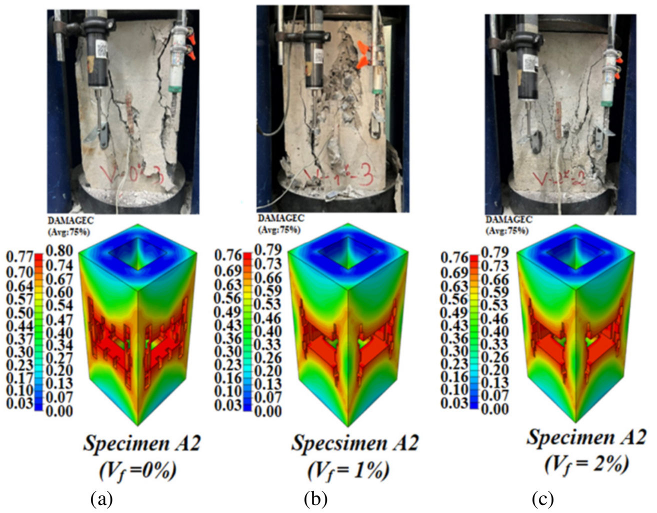

Fig. 4. Failure patterns of column A2 with varying fiber contents: (a) 0%, (b) 1%, (c) 2%.

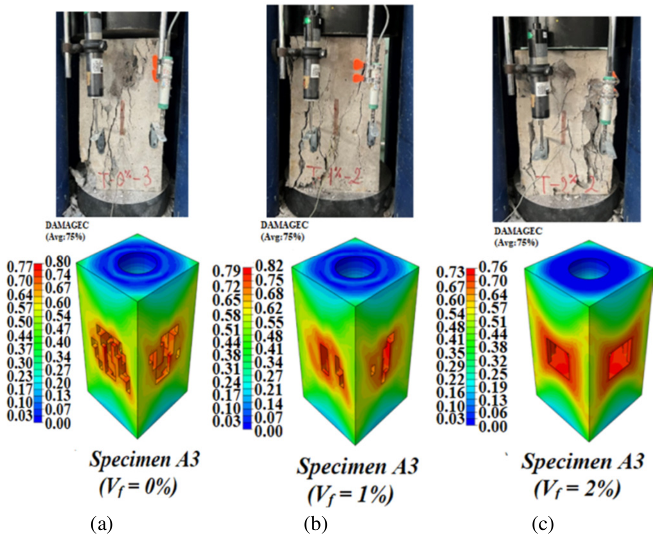

Fig. 5. Failure patterns of column A3 with varying fiber contents: (a) 0%, (b) 1%, (c) 2%.

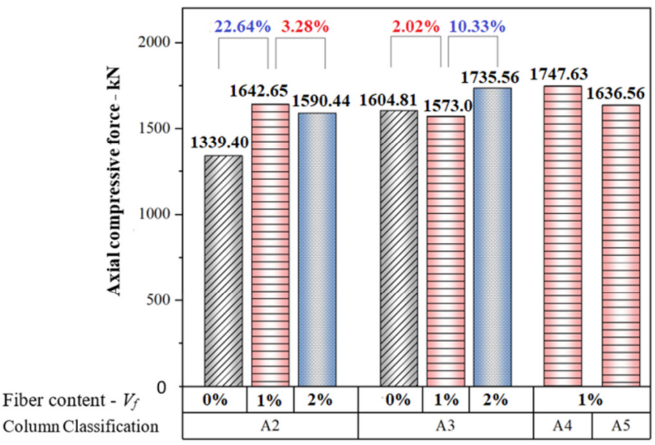

Fig. 6. Evaluation of the load-bearing capacities of different columns.

With a constant fiber content of 1%, increasing the core configuration from A2 to A4 or from A3 to A5 led to a 6.39% and 4.04% increase in compressive strength, respectively. As displayed in Figure 7, the rectangular cores outperformed the circular ones, likely due to a more balanced stress distribution. These results highlight the combined influence of fiber content and core geometry on the compressive performance of the UHPC-NSC composite structures.

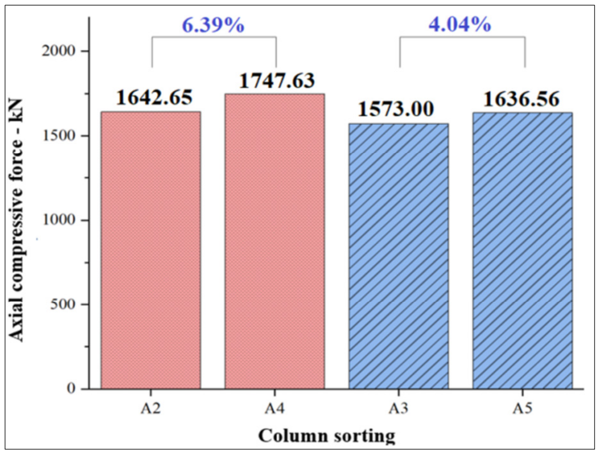

Fig. 7. Load-bearing capacity of columns with different core cross-sections, 1% fiber.

C. Load-Displacement Behavior Analysis

Figure 8 shows the load-displacement relationships of the column specimens, where N_u is the maximum compressive load and ε_u is the corresponding axial strain at peak load. All specimens exhibited a linear elastic behavior initially, followed by inelastic deformation when the load reached approximately 0.8 Nu. After reaching the peak load, the specimens exhibited degradation in the load-bearing capacity, as evidenced by a descending branch in the load-displacement curve. The specimens were categorized, as depicted in Table II, in order to analyze the influence of the material composition and core configuration on the mechanical behavior.

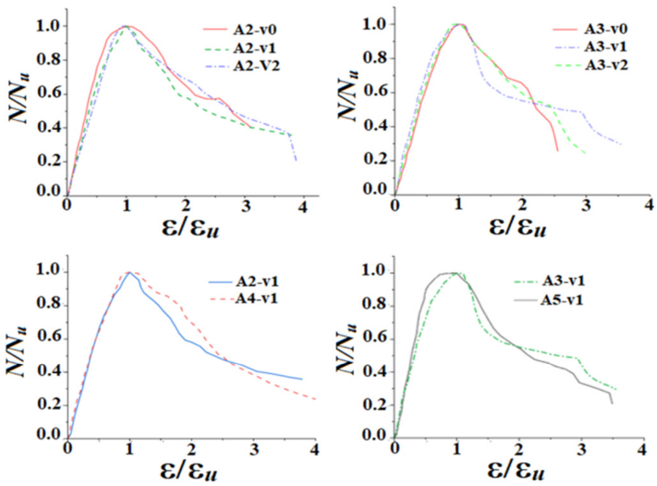

Fig. 8. Evaluation of the load-displacement curves.

TABLE II. SPECIMEN SPECIFICATIONS

Specimen type	Specimen symbol	Steel fibers	Number of Specimens	Note
A2	A2-v0-1(2,3), A2-v1-1(2,3), A2-v2-1(2,3)	0%, 1%, 2%	3, 3, 3	01 square UHPC core
A3	A3-v0-1(2,3), A3-v1-1(2,3), A3-v2-1(2,3)	0%, 1%, 2%	3, 3, 3	01 round UHPC core
A4	A4-v1-1(2,3)	1%	3	04 square UHPC core
A5	A5-v1-1(2,3)	1%	3	04 round UHPC core

The observations yielded the following findings:

- For specimen A2, an increase in the steel fiber content from 0% to 1% resulted in a notable enhancement in the compressive capacity. However, an increase to 2% resulted in a slight decrease, suggesting a potential saturation point in the effectiveness of fiber reinforcement.
- For specimen A3, increasing the fiber content from 1% to 2% resulted in a notable improvement in the load-bearing capacity. This finding indicates that the efficiency of the steel fibers may also be contingent on the geometry of the UHPC core.
- It was found that specimens A4 and A5, which featured separated UHPC cores, exhibited enhanced ductility after reaching a peak load, which is evidenced by a slower decline in the load and a greater post-peak displacement compared to specimens A2 and A3.

A comparison of the FEM simulations and experimental results, as shown in Figures 9-11, indicates that:

- Prior to reaching a peak load, the FEM models accurately predicted the load–displacement behavior.
- The post-peak discrepancies were more apparent in specimens A2 and A3, while specimens A4 and A5 exhibited a closer agreement between the experimental and simulated results.
- FEM exhibited a reliable predictive capacity for the axial compression behavior of the UHPC-NSC composite columns with varying core configurations and fiber contents.

The analysis of the load-displacement behavior indicates that the steel fiber content, the core geometry, and the distribution of the core all play critical roles in enhancing the compressive strength and post-peak performance of the UHPC-NSC composite columns.

D. Evaluation of Load Distribution on Cross-Sections

A thorough examination of the load-displacement curve illustrated in Figures 12-14, indicates that the NSC concrete accounted for up to 50% of the load-bearing capacity of column A2 and nearly 70% for the other column specimens. Specifically, the alteration of the UHPC core from a square to a circular shape resulted in an increase in the contribution ratio from 54% to nearly 70%. A subsequent comparison of the columns A4 and A5 revealed a marginal increase of approximately 4%. Consequently, the load-bearing capacity of the columns is mainly attributed to the presence of NSC concrete. An analysis of the load-displacement curve shapes indicated that when the NSC concrete reached its peak, the UHPC concrete was in the plastic deformation stage. At the point at which UHPC concrete reached its peak, the columns entered the softening phase. Despite the fact that UHPC concrete contributed only 26%–41%, the softening branch was influenced, at least in part, by the compressive strength of the UHPC concrete.

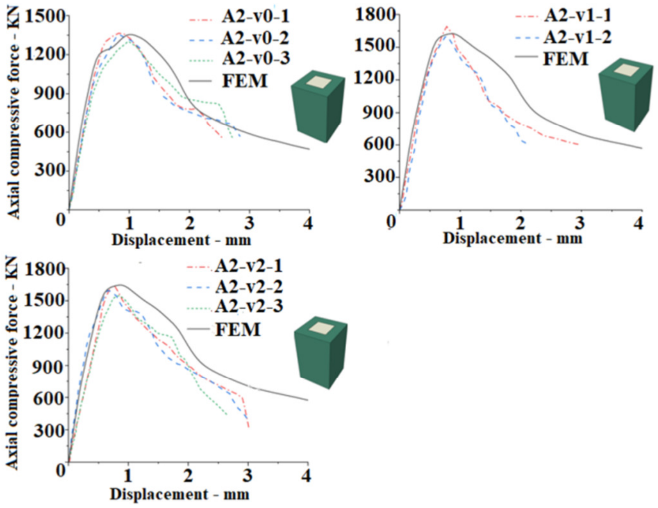

Fig. 9. Evaluation of load-displacement curve for specimen A2.

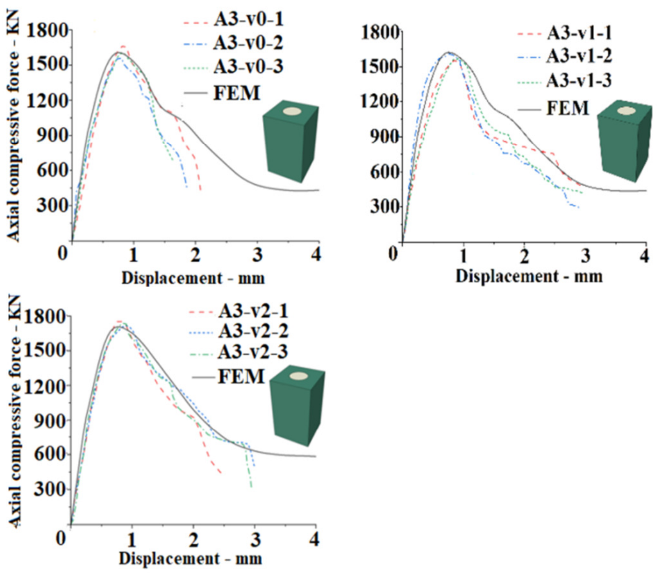

Fig. 10. Evaluation of the load-displacement curve for specimen A3.

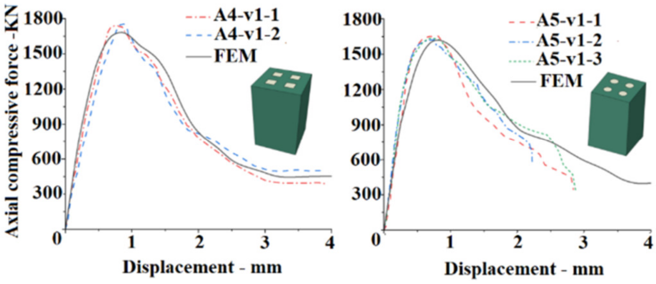

Fig. 11. Evaluation of the load-displacement curve for specimens A4-A5.

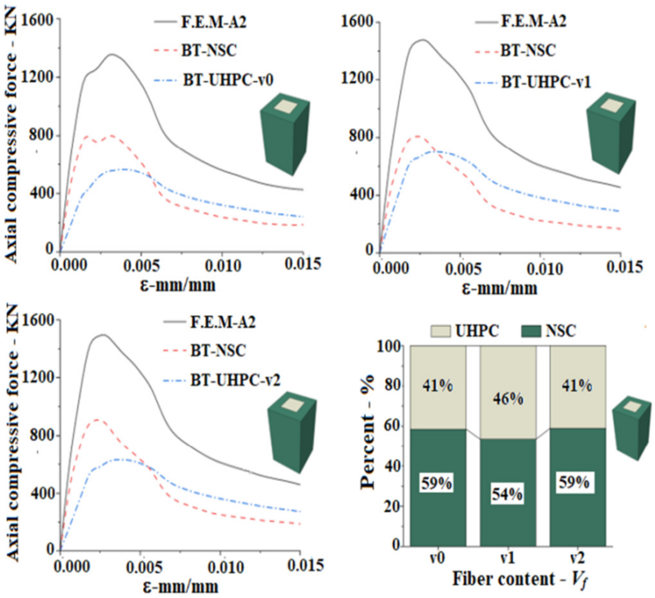

Fig. 12. Load distribution on the cross-section of specimen A2.

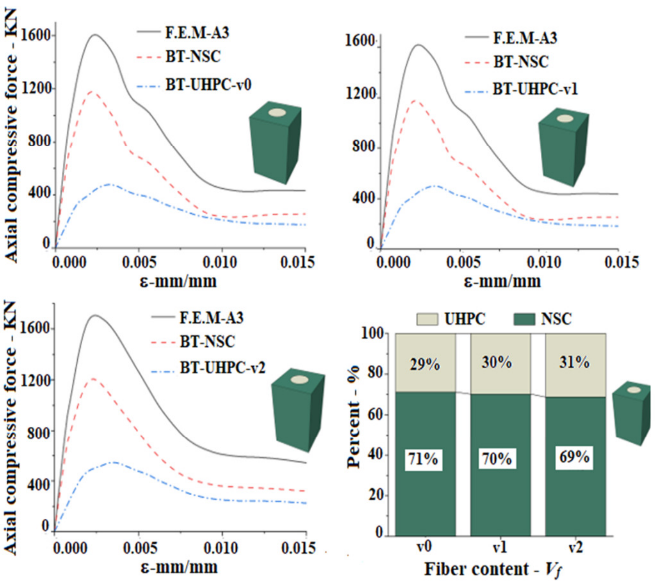

Fig. 13. Load distribution on the cross-section of specimen A3.

E. Parameter Analysis

1) Parameter Analysis Data

The data selected for the parameter analysis are shown in Table III. In this context, *H* and *B* are the constant dimensions of the column, measuring 300 mm on each side. The parameters *h*, *D*, and *b* are the sizes and shapes of the reinforcement cores. The parameter *α* is defined as the ratio of the reinforced core area to the column's cross-sectional area, $f_{c\text{-}core}$ is the compressive strength of the reinforced core concrete, and f_c is the compressive strength of the column.

2) Evaluation of the Influence of α on Compressive Capacity

The results of the load-bearing capacity evaluation for each parameter group are shown in Table VI.

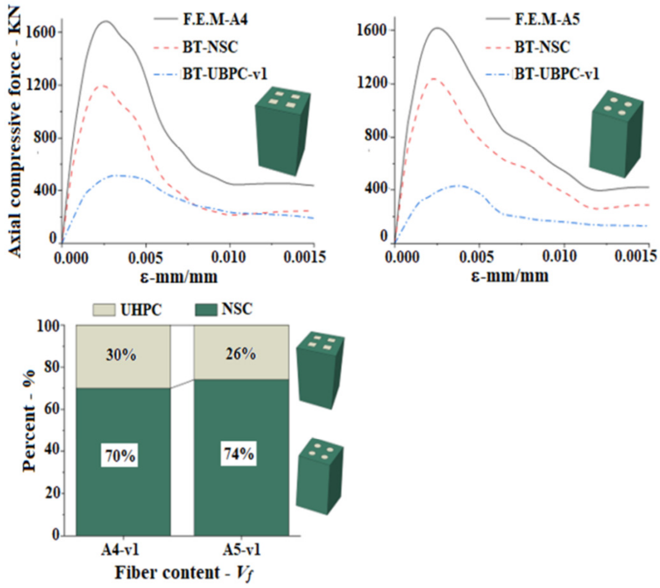

Fig. 14. Load distribution on the cross-section of specimens A4-A5.

TABLE III. PARAMETER ANALYSIS FOR CENTRALLY LOADED COLUMNS

Group	Spec. name	*H* (mm)	*B* (mm)	*h(D)* (mm)	*B* (mm)	$\alpha = \frac{A_{core}}{A_c}$	f_c (MPa)	$f_{c\text{-}core}$ (MPa)
A2	015-60	300	300	116.2	116.2	0.15	40	60
	015-90							90
	015-120							120
	030-60	300	300	164.3	164.3	0.3	40	60
	030-90							90
	030-120							120
	050-60	300	300	212.1	212.1	0.5	40	60
	050-90							90
	050-120							120
A3	015-60	300	300	131.1	-	0.15	40	60
	015-90							90
	015-120							120
	030-60	300	300	185.4	-	0.3	40	60
	030-90							90
	030-120							120
	050-60	300	300	239.4	-	0.5	40	60
	050-90							90
	050-120							120
A4	015-60	300	300	58.1	58.1	0.15	40	60

Group	Spec. name	H (mm)	B (mm)	$h(D)$ (mm)	B (mm)	$\alpha = \frac{A_{core}}{A_c}$	f_c (MPa)	$f_{c\text{-}core}$ (MPa)
	015-90							90
	015-120							120
	030-60							60
	030-90	300	300	82.2	82.2	0.3	40	90
	030-120							120
	050-60							60
	050-90	300	300	106.1	106.1	0.5	40	90
	050-120							120
A5	015-60							60
	015-90	300	300	65.6	-	0.15	40	90
	015-120							120
	030-60							60
	030-90	300	300	92.7	-	0.3	40	90
	030-120							120

TABLE IV. RESULTS OF THE COMPRESSIVE CAPACITY ANALYSIS FOR PARAMETER GROUPS

Group	Spec. name	$\alpha = \frac{A_{core}}{A_c}$	f_c (MPa)	$f_{c\text{-}core}$ (MPa)	P (MN)
A2	015-60	0.15	40	60	4.03
	015-90			90	4.37
	015-120			120	4.67
	030-60	0.3	40	60	4.20
	030-90			90	4.93
	030-120			120	5.54
	050-60	0.5	40	60	4.02
	050-90			90	5.24
	050-120			120	6.58
A3	015-60	0.15	40	60	3.98
	015-90			90	4.24
	015-120			120	4.51
	030-60	0.3	40	60	4.24
	030-90			90	4.95
	030-120			120	5.58
	050-60	0.5	40	60	4.36
	050-90			90	5.60
	050-120			120	6.87
A4	015-60	0.15	40	60	4.01
	015-90			90	4.37
	015-120			120	4.68
	030-60	0.3	40	60	4.21
	030-90			90	4.88
	030-120			120	5.50
	050-60	0.5	40	60	4.52
	050-90			90	5.69
	050-120			120	7.02
A5	015-60	0.15	40	60	2.63
	015-90			90	3.04
	015-120			120	3.41
	030-60	0.3	40	60	4.09
	030-90			90	4.79
	030-120			120	5.34

The analysis results for column groups A2-A5 exhibit variations in α, and the compressive strength of concrete. As presented in Figure 15, when the parameter α is small, enhancing the compressive strength of concrete does not result in a substantial increase in the compressive capacity of the column. Specifically, for groups A2-A4, the observed strength improvement was less than 9%. In contrast, Group A5 exhibited a range of recorded strength improvements from 12.17% to 15.58%. When $\alpha = 0.3$, the improvements became more significant in comparison to $\alpha = 0.15$. The compressive capacity of the columns exhibited an approximate 15.91% increase, reaching 17.38%, when the core compressive strength rose from 60 MPa to 90 MPa. Additionally, a 12.72% increase in compressive strength, reaching 120 MPa, was observed across all three column groups. The core area, which occupies 50% of the total cross-sectional area of the column, exhibited an increase in compressive strength, thereby enhancing the initial compressive capacity by up to 25%. For the A5 specimen, although only two ratios ($\alpha = 0.15$ and $\alpha = 0.3$) were analyzed, the results exhibited that when the core compressive strength increased from 60 MPa to 90 MPa, the compressive capacity improved by 15.58% and 17.1%, respectively. The enhancement of the core compressive strength to 120 MPa yielded a mere 12% improvement. Attaining a core compressive strength of 90 MPa is the most effective method of enhancing the column's compressive capacity. Furthermore, the usage of UHPC for the core, along with a coefficient of internal friction of 0.50, results in the optimal compressive performance for the column. Figure 16 displays that the load-displacement curves for the columns exhibit distinct behaviors. The results are categorized by column groups (A2-A5), by α, and by the compressive strength of the core concrete. The vertical axis is the ratio P/P_u, while the horizontal axis is the ratio $\varepsilon/\varepsilon_u$. Pu and ε_u represent the maximum compressive force and the corresponding maximum strain, respectively. The results indicate that only the post-peak branch is displayed ($\varepsilon/\varepsilon_u \geq 1.0$).

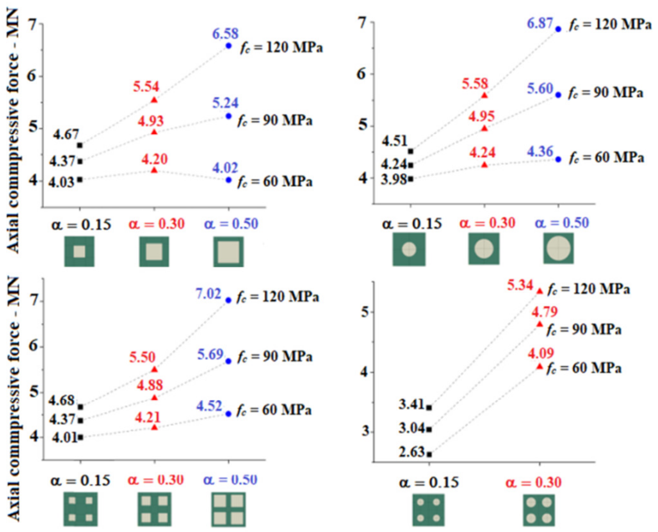

Fig. 15. Evaluation of the critical compressive force of the columns.

Findings indicate that there are no significant changes in the post-peak branch shapes for the columns in groups A3 and A5. However, substantial variations in the post-peak branch shapes were observed for the columns in groups A2 and A4. For group A2, the slope of the post-peak branch is influenced by the ratio α and the compressive strength of the core concrete. Higher α ratios exhibit an inverse correlation with the slope of the post-peak branch. Furthermore, lower-strength concrete has been observed to demonstrate a greater propensity for the ductile behavior in comparison to UHPC. For group A4, no significant differences were observed among the columns with α = 0.15. However, columns with α = 0.30 exhibited a behavior analogous to that of group A2. In other cases, different patterns emerged, and at a compressive strength of 90 MPa, the behavior tended to converge toward similar shapes.

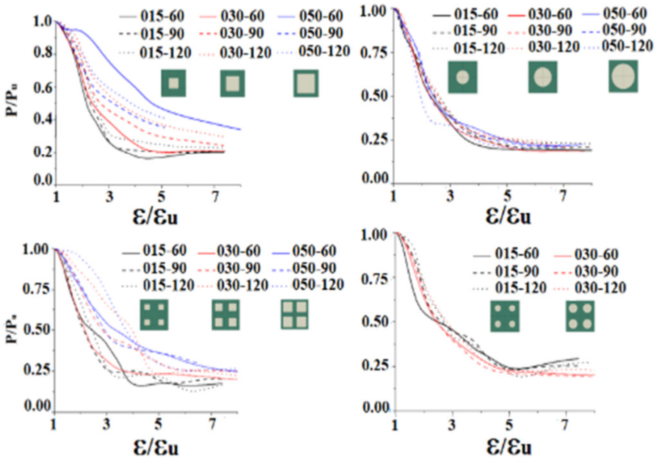

Fig. 16. Evaluation of load-displacement curves.

IV. CONCLUSIONS

This study used three-dimensional finite element simulations and experimental validation to examine the axial compressive behavior of Ultra-High-Performance Concrete–Normal-Strength Concrete (UHPC-NSC) composite columns with various core configurations. From the analysis it can be concluded that:

- The addition of 1% steel fibers to the UHPC core resulted in a substantial enhancement of the maximum compressive strength of the composite columns. This enhancement varied between 10% and 22%, depending on the configuration of the core. However, the fiber content exhibited a negligible effect on altering the overall failure modes and crack propagation patterns. This finding explains the observed phenomenon in which the load-bearing capacity increased, while the fundamental failure behavior remained largely unchanged.
- The selection of a steel fiber volume fraction of 1% (vf = 1%) was made on the basis of prior research identifying this value as optimal in balancing the mechanical performance and workability [1]. Nonetheless, the present study acknowledges the limitation of analyzing only a single fiber content and proposes that future studies consider a broader range (e.g., 0.5%, 1.5%, 2%) to better capture the nonlinear fiber-matrix interactions, particularly under post-peak loading conditions.
- A comparative analysis of three columns was conducted, each containing rectangular UHPC cores. The study revealed that the columns with rectangular cores exhibited a superior compressive performance in comparison to those with circular cores. This phenomenon was primarily attributed to a more uniform stress distribution and reduced stress concentrations at the edges. The finite element stress analyses confirmed that the incorporation of rectangular cores led to enhanced load transfer paths and delayed the formation of plastic hinges, thereby enhancing the structural efficiency.
- As indicated by both the experimental and numerical findings, the UHPC-NSC composite columns exhibited an augmented post-peak ductility in comparison to the conventional NSC columns. Quantitative metrics, such as the strain at 80% of peak load (ε_{80}%) and energy absorption capacity, were employed to assess the specimens. The results indicated that the specimens with separated UHPC cores (A4, A5) exhibited 15%-25% higher energy absorption compared to those with solid cores, suggesting a superior toughness.
- The load-sharing mechanism between NSC and UHPC proved to be a critical factor in the overall behavior of the composite columns. During the elastic and early inelastic stages, the NSC shell provided a significant contribution to the global stiffness and initial load-bearing capacity. As the loading process unfolded, the UHPC core progressively engaged, impeding the extension of cracks and offering substantial resistance to tensile forces. This collaborative interaction increased both the strength and ductility in comparison to the NSC columns when used separately.
- Despite the encouraging outcome, this study is not without its limitations. The restriction of the range of fiber contents examined, which is a key element in the analysis, is a primary concern. Additionally, the absence of a detailed assessment of plastic hinge development under combined loading conditions is a notable omission. In the future, researchers should consider expanding the range of the fiber volumes studied, diversifying the core geometries, and conducting in-depth analyses of the load-sharing and failure mechanisms. These efforts would optimize the design of UHPC-NSC composite columns for practical engineering applications.

ACKNOWLEDGEMENT

The authors would like to gratefully acknowledge the support of Tra Vinh University and Ho Chi Minh City University of Transport in this study.

REFERENCES

[1] T. V. Nguyen, T. A. Nguyen, and A. H. Le, "An Experimental Study on the Axial Compressive Behavior of Normal Concrete Composite Square Columns with UHPC Internal Cores," *Engineering, Technology & Applied Science Research*, vol. 15, no. 2, pp. 22065–22071, Apr. 2025, https://doi.org/10.48084/etasr.10146.

[2] T. Makita and E. Brühwiler, "Tensile fatigue behaviour of Ultra-High Performance Fibre Reinforced Concrete combined with steel rebars (R-UHPFRC)," *International Journal of Fatigue*, vol. 59, pp. 145–152, Feb. 2014, https://doi.org/10.1016/j.ijfatigue.2013.09.004.

[3] D.-Y. Yoo and N. Banthia, "Mechanical properties of ultra-high-performance fiber-reinforced concrete: A review," *Cement and Concrete Composites*, vol. 73, pp. 267–280, Oct. 2016, https://doi.org/10.1016/j.cemconcomp.2016.08.001.

[4] X.-B. Luu and S.-K. Kim, "Finite Element Modeling of Interface Behavior between Normal Concrete and Ultra-High Performance Fiber-Reinforced Concrete," *Buildings*, vol. 13, no. 4, Apr. 2023, Art. no. 950, https://doi.org/10.3390/buildings13040950.

[5] T. Tong, S. Yuan, J. Wang, and Z. Liu, "The role of bond strength in structural behaviors of UHPC-NC composite beams: Experimental investigation and finite element modeling," *Composite Structures*, vol. 255, Jan. 2021, Art. no. 112914, https://doi.org/10.1016/j.compstruct.2020.112914.

[6] J. Yu, B. Zhang, W. Chen, H. Liu, and H. Li, "Multi-scale study on interfacial bond failure between normal concrete (NC) and ultra-high performance concrete (UHPC)," *Journal of Building Engineering*, vol. 57, Oct. 2022, Art. no. 104808, https://doi.org/10.1016/j.jobe.2022.104808.

[7] M. A. Sakr, B. Osama, and T. M. El Korany, "Modeling of ultra-high performance fiber reinforced concrete columns under eccentric loading," *Structures*, vol. 32, pp. 2195–2210, Aug. 2021, https://doi.org/10.1016/j.istruc.2021.04.026.

[8] A. M. T. Hassan, S. W. Jones, and G. H. Mahmud, "Experimental test methods to determine the uniaxial tensile and compressive behaviour of ultra high performance fibre reinforced concrete (UHPFRC)," *Construction and Building Materials*, vol. 37, pp. 874–882, Dec. 2012, https://doi.org/10.1016/j.conbuildmat.2012.04.030.

[9] E. J. Mezquida-Alcaraz, J. Navarro-Gregori, J. Á. Lopez, and P. Serna-Ros, "Validation of a non-linear hinge model for tensile behavior of UHPFRC using a Finite Element Model," *Computers and Concrete*, vol. 23, no. 1, pp. 11–23, Jan. 2019.

[10] M. A. Sakr, T. M. El Korany, and B. Osama, "Analysis of RC columns strengthened with ultra-high performance fiber reinforced concrete jackets under eccentric loading," *Engineering Structures*, vol. 220, Oct. 2020, Art. no. 111016, https://doi.org/10.1016/j.engstruct.2020.111016.

[11] M. Elchalakani, A. Karrech, M. Dong, M. S. Mohamed Ali, and B. Yang, "Experiments and Finite Element Analysis of GFRP Reinforced Geopolymer Concrete Rectangular Columns Subjected to Concentric and Eccentric Axial Loading," *Structures*, vol. 14, pp. 273–289, Jun. 2018, https://doi.org/10.1016/j.istruc.2018.04.001.

[12] B. Osama and M. Sakr, "Modeling of Ultra-high Performance Fiber Reinforced Concrete Filled Steel Tube Columns under Eccentric Loading," *Periodica Polytechnica Civil Engineering*, vol. 67, no. 1, pp. 10–23, Jan. 2023, https://doi.org/10.3311/PPci.20593.

[13] M. Mursi and B. Uy, "Strength of Concrete Filled Steel Box Columns Incorporating Interaction Buckling," *Journal of Structural Engineering*, vol. 129, no. 5, pp. 626–639, May 2003, https://doi.org/10.1061/(ASCE)0733-9445(2003)129:5(626).

[14] M. Mursi and B. Uy, "Strength of slender concrete filled high strength steel box columns," *Journal of Constructional Steel Research*, vol. 60, no. 12, pp. 1825–1848, Dec. 2004, https://doi.org/10.1016/j.jcsr.2004.05.002.

[15] K. Sakino, H. Nakahara, S. Morino, and I. Nishiyama, "Behavior of Centrally Loaded Concrete-Filled Steel-Tube Short Columns," *Journal of Structural Engineering*, vol. 130, no. 2, pp. 180–188, Feb. 2004, https://doi.org/10.1061/(ASCE)0733-9445(2004)130:2(180).

[16] Z. Huang, D. Li, B. Uy, H.-T. Thai, and C. Hou, "Local and post-local buckling of fabricated high-strength steel and composite columns," *Journal of Constructional Steel Research*, vol. 154, pp. 235–249, Mar. 2019, https://doi.org/10.1016/j.jcsr.2018.12.004.

[17] T. Zhang, F. Ding, X. Liu, and Z. Yu, "Compressive behavior of steel-reinforced concrete-filled circular steel tubular stub columns," *Structures*, vol. 28, pp. 863–877, Dec. 2020, https://doi.org/10.1016/j.istruc.2020.08.012.

[18] *Abaqus analysis user's manual*. Dassault Systèmes Simulia Corp., 2014.

[19] V. K. Papanikolaou and A. J. Kappos, "Confinement-sensitive plasticity constitutive model for concrete in triaxial compression," *International Journal of Solids and Structures*, vol. 44, no. 21, pp. 7021–7048, Oct. 2007, https://doi.org/10.1016/j.ijsolstr.2007.03.022.

[20] P. E. C. Seow and S. Swaddiwudhipong, "Failure Surface for Concrete under Multiaxial Load—a Unified Approach," *Journal of Materials in Civil Engineering*, vol. 17, no. 2, pp. 219–228, Apr. 2005, https://doi.org/10.1061/(ASCE)0899-1561(2005)17:2(219).

[21] T. Yu, J. G. Teng, Y. L. Wong, and S. L. Dong, "Finite element modeling of confined concrete-I: Drucker–Prager type plasticity model," *Engineering Structures*, vol. 32, no. 3, pp. 665–679, Mar. 2010, https://doi.org/10.1016/j.engstruct.2009.11.014.

[22] L. D. Tolentino, V. B. dos Santos, B. L. Poncetti, R. M. Enami, P. A. Krahl, and R. D. Vanderlei, "Effect of ultra-high performance concrete repair layer thickness on the behavior of concrete columns," *Structural Concrete*, vol. 25, no. 3, pp. 1801–1818, 2024, https://doi.org/10.1002/suco.202300165.

[23] J. Xie, Q. Fu, and J.-B. Yan, "Compressive behaviour of stub concrete column strengthened with ultra-high performance concrete jacket," *Construction and Building Materials*, vol. 204, pp. 643–658, Apr. 2019, https://doi.org/10.1016/j.conbuildmat.2019.01.220.

[24] B. De Nicolo, L. Pani, and E. Pozzo, "Strain of concrete at peak compressive stress for a wide range of compressive strengths," *Materials and Structures*, vol. 27, no. 4, pp. 206–210, May 1994, https://doi.org/10.1007/BF02473034.

[25] B. Wahalathantri, D. Thambiratnam, T. Chan, and S. Fawzia, "A material model for flexural crack simulation in reinforced concrete elements using ABAQUS," in *Proceedings of the First International Conference on Engineering, Designing and Developing the Built Environment for Sustainable Wellbeing*, C. J. L. Cowled, Ed. Australia: Queensland University of Technology, 2011, pp. 260–264.

[26] Z. P. Bažant and E. Becq-Giraudon, "Statistical prediction of fracture parameters of concrete and implications for choice of testing standard," *Cement and Concrete Research*, vol. 32, no. 4, pp. 529–556, Apr. 2002, https://doi.org/10.1016/S0008-8846(01)00723-2.

[27] D. J. Carreira and K.-H. Chu, "Stress-Strain Relationship for Plain Concrete in Compression," *Journal Proceedings*, vol. 82, no. 6, pp. 797–804, Nov. 1985, https://doi.org/10.14359/10390.